Surface & Coatings Technology 206 (2012) 2914–2921

Contents lists available at SciVerse ScienceDirect

Surface & Coatings Technology

journal homepage: www.elsevier.com/locate/surfcoat

Dual Ti and C ion-implanted stainless steel bipolar plates in polymer electrolyte membrane fuel cells

Kai Feng [a,b], Guosong Wu [b], Tao Hu [b], Zhuguo Li [a,*], Xun Cai [a,**], Paul K. Chu [b,***]

[a] Shanghai Key laboratory of Materials Laser Processing and Modification, School of Materials Science and Engineering, Shanghai Jiao Tong University, Shanghai 200240, China
[b] Department of Physics and Materials Science, City University of Hong Kong, Tat Chee Avenue, Kowloon, Hong Kong, China

ARTICLE INFO

Article history:
Received 5 July 2011
Accepted in revised form 15 December 2011
Available online 26 December 2011

Keywords:
Ion implantation
Titanium
Carbon
Corrosion resistance
Electrical conductivity
Bipolar plates

ABSTRACT

The effects of dual Ti and C ion implantation on the corrosion resistance and surface conductivity of 316L stainless steel (SS) bipolar plates used in polymer electrolyte membrane fuel cells (PEMFC) are investigated. The ion-implanted SS bipolar plates are assembled into single cells to evaluate the performance and improvement. X-ray photoelectron spectroscopy (XPS) confirms the presence of the implanted layer and high-resolution transmission electron microscopy (HR-TEM) discloses an amorphous phase together with an underlying layer with fine grains on the surface of the Ti0.5C0.5 specimen due to ion collision. On the other hand, the surface microstructure of Ti0.5C2 consists of a precipitated nanophase layer, an amorphous underlying layer, and a zone with refined grains between the implanted surface and substrate. The interfacial contact resistance (ICR) of Ti0.5C0.5 is reduced by 6.5 times due to the Ti and C enriched surface and amorphous and fine grain underlayer. Electrochemical characterization and scanning electron microscopy (SEM) show reduced current density and improved corrosion resistance as a result of implantation of a proper ion fluence. According to the single cell evaluation, the peak power density of the ion-implanted bipolar plate increases from 566.5 mW cm^{-2} to 709.8 mW cm^{-2} and the power density at 0.6 V increases by about 50% compared to those measured from the single cell assembled with unimplanted SS bipolar plates.

1. Introduction

Stainless steels are potential bipolar plate materials in polymer electrolyte membrane fuel cells (PEMFC) because of the good mechanical strength, high electrical conductivity, high gas impermeability, low cost, and easy manufacturing processes [1,2]. However, stainless steel has its inherent shortcomings in the weakly acidic PEMFC electrolyte containing ions such as F^-, SO_4^{2-}, Cl^-, etc. [3]. In this environment, the corrosion resistance of stainless steel is not sufficient thereby compromising the durability and lifetime of PEM fuel cells [4–6]. In addition, stainless steel is usually covered by a passive film which significantly increases the interfacial contact resistance (ICR) between the bipolar plates and carbon paper. In this respect, surface modification can increase the corrosion resistance and surface electrical conductivity. In a recent review, Antunes et al. [5] summarize the surface modification methods and results acquired from metallic bipolar plates and point out that incorporation of elements capable of enhancing the corrosion resistance and electrical conductance is the best choice. Lavigne et al. [7] apply electrochemical treatment to insert cerium in 316L stainless steel passive film to improve the conductivity and corrosion resistance. The results show the corrosion resistance and conductivity are improved by cerium treatment. Ion implantation is an excellent surface modification technique and has been used on various materials to improve the surface properties [8–12]. In ion implantation, the distribution and concentration of the implanted elements can be tailored without restriction of solubility and phase diagrams [13]. Other benefits include no change of sample shape, flexible processing temperature, good adhesion between the modified layer and substrate due to ion mixing, and environmental friendliness. Zhang et al. [14] studies the effect of Ti + C dual implantation on the hardness of H13 steel and find dispersion hardening phases of Fe_2Ti and TiC. In another study, they investigate the corrosion behavior of Ti + C implanted H13 steel. The corrosion current density of Ti + C dual implanted steel is greatly decreased and being 1.2% of that of non-implanted samples [15]. Carbon ion implantation is used to modify the surface of Ni-based amorphous alloys as bipolar plate in PEMFC [16]. The results indicate carbon ion implanted Ni-based amorphous alloy has corrosion resistance as well as graphite and the contact resistance is decreased to a level comparable to that of graphite. Previous work by Weng, et al., showed that ion implantation of Ti into Type 304 stainless steel decreased the open circuit corrosion rate in 0.5 M H_2SO_4 and decreased both the critical current density for passivation and the passive current density [17]. Ion implantation of Ti into 52100 steel improved the corrosion resistance in H_2SO_4 solutions and in chloride solution due

* Corresponding author. Tel.: +86 21 54748940; fax: +86 21 34203024.
** Corresponding author. Tel.: +86 21 54748940; fax: +86 21 62182903.
*** Corresponding author. Tel.: +852 34427724; fax: +852 34420542.
E-mail addresses: lizg@sjtu.edu.cn (Z. Li), xcai@sjtu.edu.cn (X. Cai), paul.chu@cityu.edu.hk (P.K. Chu).

0257-8972/$ – see front matter.
doi:10.1016/j.surfcoat.2011.12.021

to the formation of a Fe–Ti–C amorphous surface [18]. In this work, we conduct dual Ti and C ion implantation to improve the corrosion resistance and surface electrical conductivity of stainless steels and the performance of the ion-implanted and control SS bipolar plates is compared.

2. Experimental details

Stainless steel 316L (SS316L) samples (16.4 at.% Cr, 8.2 at.% Ni, and 2.0 at.% Mo, balance being Fe) were used in our experiments. The specimens were polished with SiC waterproof abrasive paper up to #1200, degreased with acetone, cleaned with alcohol in an ultrasonic cleaner, and dried prior to ion implantation and subsequent tests. Ion implantation was carried out on the HEMII-80 High Energy Metal Ion Implanter manufactured by Plasma Technology Limited as shown in Fig. 1. The vacuum in the implantation chamber was below 5.0×10^{-5} Pa. Titanium ion was first implanted at an accelerating voltage of 20 kV for 0.5 h and the ion implant fluence is calculated according to the following formula:

$$D\left(ions/cm^2\right) = k\frac{I_m\cdot\tau\cdot n}{e\cdot S\cdot\overline{n_0}}, \quad (1)$$

in which k is the empirical coefficient usually between 0.30 and 0.35, I_m is the average current, τ is the pulse width being 1 ms, n is pulse number, e is electron charge, S is ion beam area, and $\overline{n_0}$ is the average charge state number. As the average charge state number of titanium is +2.1 [19], the calculated ion implant fluence after implantation for 0.5 h is about 3×10^{16} ions cm^{-2}. The samples then underwent carbon implantation at 40 kV for 0.25 h, 0.5 h, 1 h, or 2 h. Taking the average charge state number of carbon of +1 [19], the calculated ion implant fluences are about 6×10^{16} ions-cm^{-2}, 1.2×10^{17} ions-cm^{-2}, 2.4×10^{17} ions-cm^{-2}, and 4.8×10^{17} ions-cm^{-2} for Ti0.5C0.25, Ti0.5C0.5, Ti0.5C1 and Ti0.5C2, respectively where the last number designates the carbon implantation time.

Table 1
Main operating conditions in the single cell test.

Parameter	Cathode side	Anode side
Active area	40 cm^2	40 cm^2
Reactant flow rate	1200 SCCM (O_2)	1000 SCCM (H_2)
Back pressure	50 kPa	30 kPa
Humidification	30%	30%
Cell temperature	52 °C	52 °C
Reactant temperature	60 °C	60 °C

X-ray photoelectron spectroscopy (XPS) was conducted on the Physical Electronics PHI 5802 equipped with a monochromatic Al K_α source to determine the elemental depth profiles in the near surface of the bare and ion implanted SS316L. The surface chemical composition and depth profiles were determined by using a constant pass energy of 11.75 eV and the photoelectrons were collected at a take-off angle of 45° with a step size of 0.25 eV. The cross-sectional microstructure of the implanted SS316L samples was examined by high-resolution transmission electron microscopy (HR-TEM) using a Philips F20 microscope operated at 200 kV.

The interfacial contact resistance (ICR) of the bare and implanted SS316L samples were evaluated on a structure with two pieces of conductive carbon paper (Toray TGP-H-090) sandwiched between the sample and two copper plates. A constant current of 0.1 A was applied through the two copper plates and the voltage was monitored as a

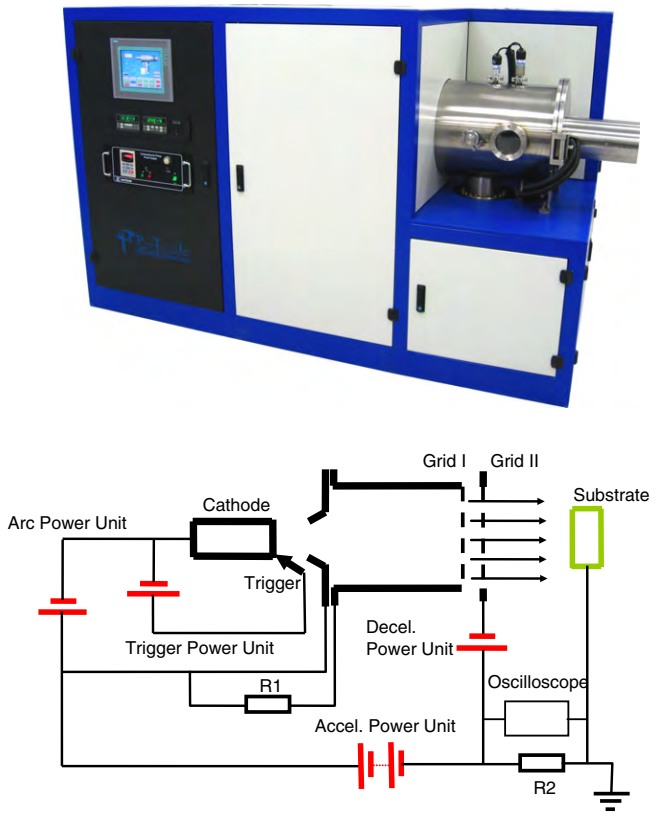

Fig. 1. Photo and schematic diagram of HEMII-80 high energy metal ion implanter.

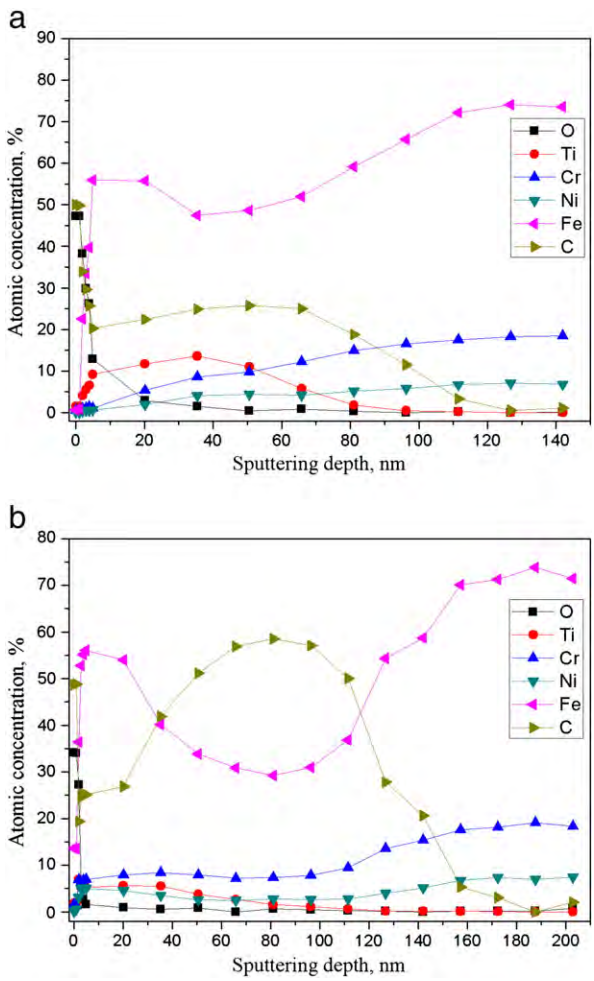

Fig. 2. XPS depth profiles: (a) Ti0.5C0.25 and (b) Ti0.5C2.

function of the steadily increasing compaction force. The ICR between the carbon paper and copper plate was subtracted for calibration and so the results reported here represent the corrected ICR values between the sample and carbon paper.

In order to investigate the electrochemical behavior and surface passivation, potentiodynamic and potentiostatic tests were conducted. The electrochemical tests were carried out on a Zahner Zennium Electrochemical Workstation. A conventional three-electrode system in which the platinum sheet was the counter electrode, the saturated calomel electrode (SCE) served as the reference electrode, and the sample as the working electrode was adopted. The electrochemical tests were carried out in a common PEMFC accelerated solution [20–22] containing 0.5 M H_2SO_4 and 2 ppm HF at 80 °C. The solution was aspirated thoroughly by either hydrogen gas (simulating the anode environment) or air (cathode environment) before and during the electrochemical test. The open circuit potential (OCP) versus time relationship was recorded for 1 h and then the potentiodynamic polarization was monitored in the anodic direction at a sweeping rate of 1 mV s^{-1}. The potentiostatic test was conducted for 10 h at polarized potentials of 0.6 V and −0.1 V in the simulated PEMFC cathode and anode environment [23,24], respectively to study the corrosion rate and stability. 100 ml of the solution were collected after the potentiostatic test and analyzed by inductively-coupled plasma atomic emission spectrometry (ICP-AES) to determine the concentrations of Fe, Cr, Ni, Mo and Ti. The surface topography of the ion implanted SS316L after the electrochemical tests was studied by scanning electron microscopy (SEM, JEOL JSM-820).

A home-made single cell was designed and fabricated to evaluate the single cell performance of the samples. According to the surface conductivity and corrosion resistance results, Ti 0.5 h and C 0.5 h were selected as the optimal conditions to modify the 0.1 mm thick SS316L bipolar plates. Commercial MEA (anode) with platinum (cathode) loading of 0.5 mg cm^{-2} and an active electrode area of 40 cm^2 were adopted. Aluminum plates 15 mm thick were used as the end plates and 2 mm thick brass plates collected the current. The coated bipolar plates, MEAs, silicon seals, and current collectors were clamped between the two end plates by eight M4 screw joints at a torque of about 6 Nm. The single cell test was carried out under the I–V mode in the NBT-100W fuel cell test system. The experiments were carried out under the scanning current mode and the results were recorded after 2 h of stable operation. The important instrumental parameters are listed in Table 1.

3. Results and discussion

The XPS depth profiles of Fe, Cr, Ni, O, Ti and C in the implanted SS316L are shown in Fig. 2. Fig. 2(a) acquired from Ti0.5C0.5 evinces

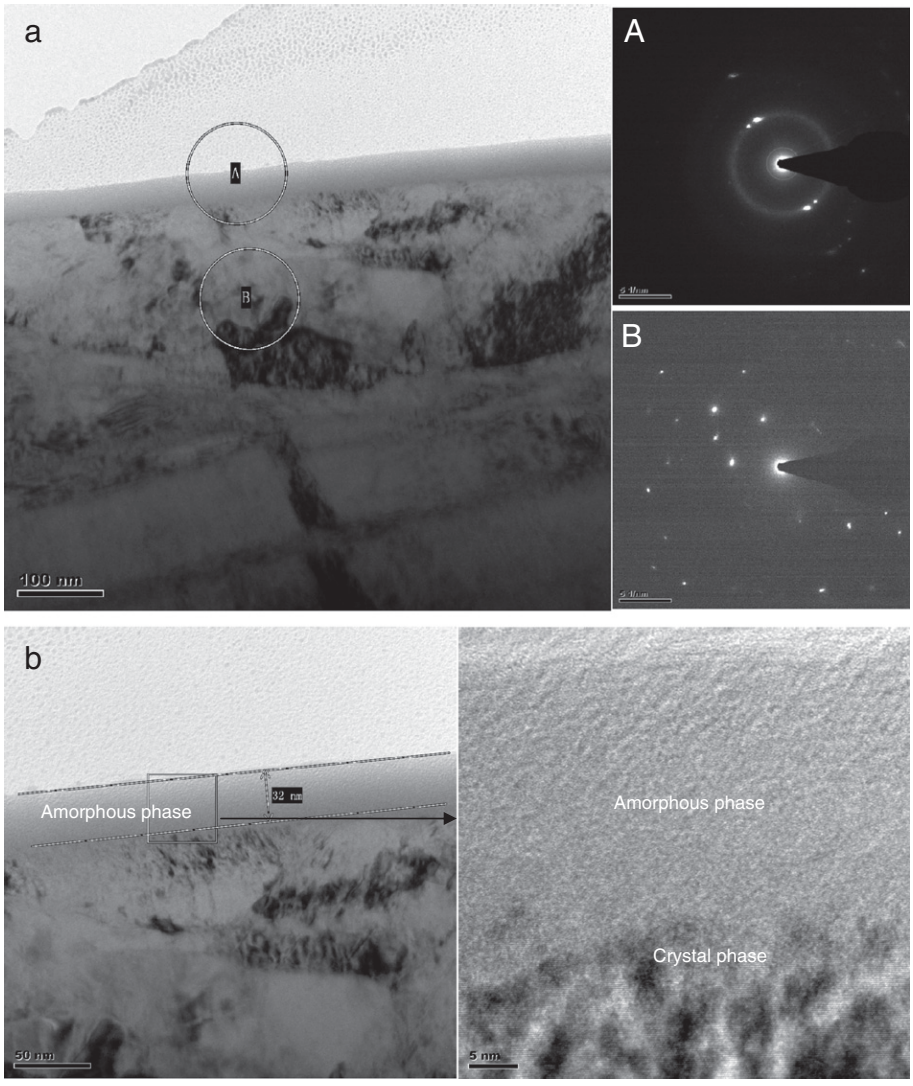

Fig. 3. HR-TEM cross-sectional microstructure of Ti0.5C0.5.

10–15 at.% Ti from 5 to 50 nm and more than 20 at.% C from 5 to 70 nm. As the average impact energy of titanium is 42 keV (20 keV×2.1) whereas the average energy of carbon is 40 keV (40 keV×1), the penetration of carbon is deeper also due to the smaller mass. The depth profile of Ti0.5C2 in Fig. 2(b) reveals that the carbon concentration increases to 55 at.% at the peak but the titanium concentration is smaller. At the same time, the Fe concentration is greatly reduced around the carbon peak but the Ti concentration is not, indicating that carbon and titanium substitute for iron in the implanted samples.

The cross-sectional microstructure of the Ti and C implanted samples Ti0.5C0.5 and Ti0.5C2 is examined by HR-TEM and the results are depicted in Figs. 3 and 4, respectively. An amorphous layer with an approximate thickness of 32 nm is formed on the surface of Ti0.5C0.5 due to radiation damage as indicated by the selected area diffraction (SAD) spectrum obtained from area A. Formation of the amorphous layer in conjunction with the compact structure and fine grains under this layer mitigates the adverse effect of the heterogeneous surface and improves the corrosion resistance. Fig. 4 shows the HR-TEM cross-sectional microstructure of Ti0.5C2. There is a surface layer about 36 nm thick containing precipitated nanophases as shown in area D in Fig. 4(b) caused by an overdose in C ion implantation. The SAD corresponding to area A shows the diffraction rings superimposed by diffraction spots stemming from the electron diffraction in the nanocrystalline structure. The precipitated nanophase is chromium carbide and iron carbide as determined from previous studies involving co-implantation of V and C [25], Nb

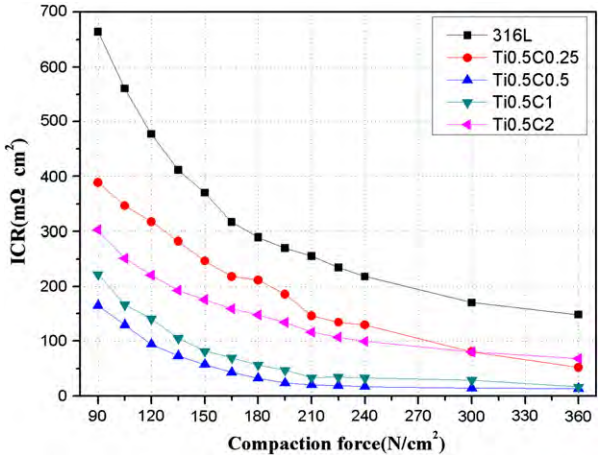

Fig. 5. ICR values of the bare and Ti and C implanted SS316L samples versus compaction force.

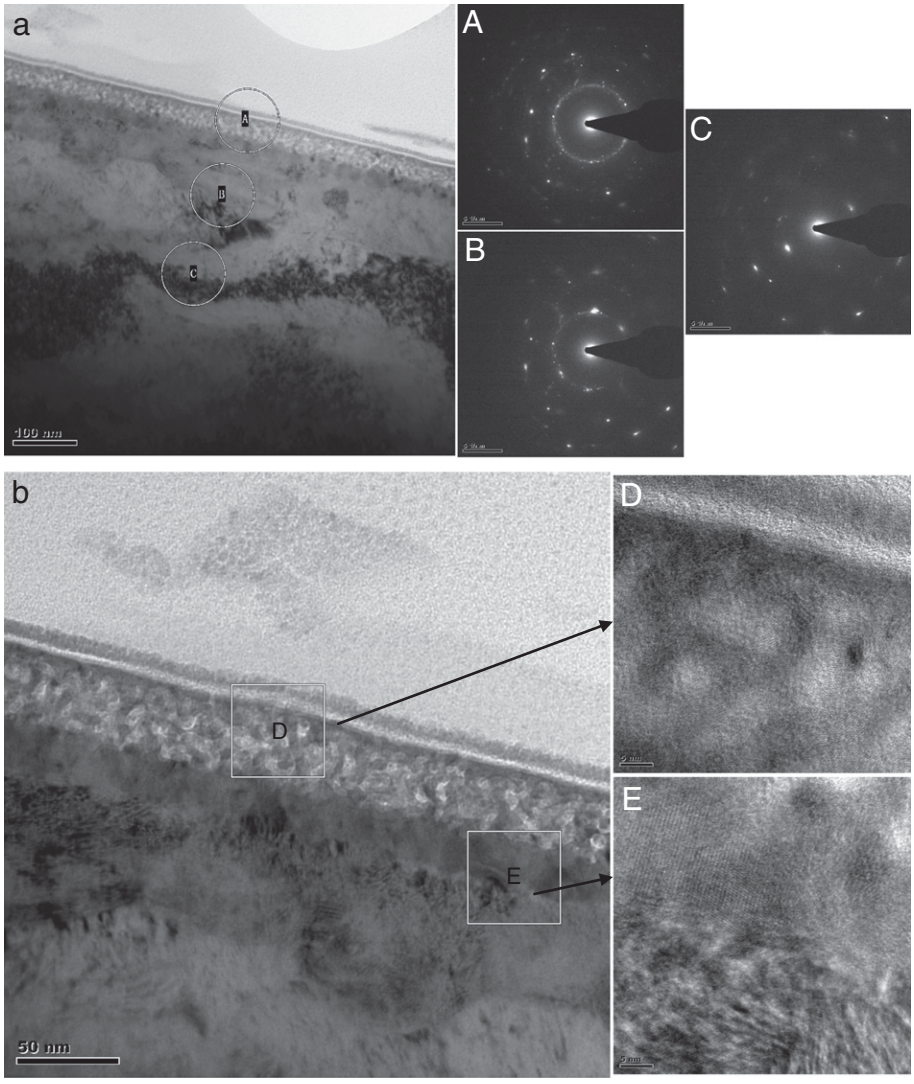

Fig. 4. HR-TEM cross-sectional microstructure of Ti0.5C2.

and C [26], as well as Ti and C [15]. Underneath an amorphous phase about 22.6 nm in thickness can be seen in Fig. 4(b) [area E]. The diffraction pattern in area C shows traces of the austenite γ phase from depth of 200 to 300 nm.

The ICR between the implanted and unimplanted samples and carbon paper is shown in Fig. 5 as a function of compaction force. In general, the ICR decreases with compaction force exponentially, indicating that the compaction force is dominant in the low compaction force region whereas the surface composition is predominant in the other region. The ICR of bare SS316L is 370 mΩ cm^2 at a typical compaction force of 150 N cm^{-2} due to the formation of passive film on the surface. After Ti + C dual implantation, the ICR of all samples decrease due to the enrichment of titanium and carbon element and thinner passive film caused by sputtering effect during ion implantation. In specific, the ICR of Ti0.5C0.25 being lower than that of SS316L is 246 mΩ cm^2. When the implant fluence ratio of titanium and carbon reaches 1:1 (that is, sample Ti0.5C0.5), the ICR exhibits the lowest value of being 57 mΩ cm^2 at the typical compaction force. When the carbon implant fluence is higher, ICR increases with fluence. However, in another study [27], we find that the ICR of carbon implanted SS316L decreases with increasing implantation fluence due to the precipitation graphite nanophase in high implantation fluence. The lowest ICR is obtained when implanted for 2 h and reaches 127.8 mΩ cm^2, much higher than that of Ti0.5C0.5 sample. The improved surface conductivity of SS316L due to Ti and C ion implantation implies that the internal resistance of the PEMFC stack can be substantially reduced to enhance the output power density.

The potentiodynamic polarization test results conducted in 0.5 M H_2SO_4 + 2 ppm HF solution at 80 °C are presented in Fig. 6. As shown by Fig. 6(a), the corrosion potential of the implanted specimens is more positive than that of the unimplanted one and the passive current density is smaller. In particular, the corrosion potential of SS316L is −265 mV and the passive current density at the cathode operation potential is 17.9 μA cm^{-2}. In comparison, the corrosion potential of Ti0.5C0.5 is 153 mV and the passive current density at 0.6 V is 6.0 μA cm^{-2}. Thermodynamically, a higher corrosion potential means higher chemical inertness and less corrosion tendency. The carbon ion implantation also improves the corrosion resistance of SS316L in cathode environment. For C implanted 2 h sample, the corrosion potential is 65 mV and the passive current density at 0.6 V is 4.0 μA cm^{-2}. Although the passive current density of Ti + C dual implanted SS316L at 0.6 V is little higher than that of C implanted sample, the surface conductivity of Ti0.5C0.5 sample exhibits obvious advantage. In the simulated anode environment, the corrosion potential (E_{corr}) of the bare SS316L is close to −271 mV and the anode operation potential (about −0.1 V) is in the passive region as shown in Fig. 6(b). After Ti and C ion implantation, the corrosion potential shifts towards the positive direction and is more positive than the anode operation potential. Sample Ti0.5C0.5 exhibits the most positive corrosion potential of 272 mV. The potentiodynamic polarization results indicate that the corrosion rate is significantly diminished by Ti and C ion implantation.

Under the PEMFC working conditions, the bipolar plate is not usually corroded at the free corrosion potential but rather the applied

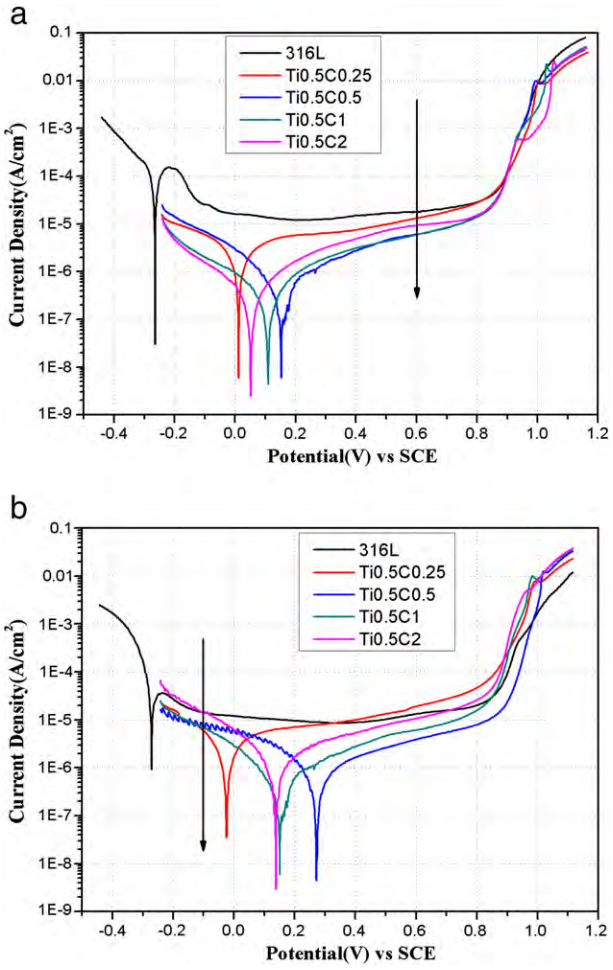

Fig. 6. Potentiodynamic curves obtained from the bare and Ti and C implanted SS316L samples in 0.5 M H_2SO_4 + 2 ppm HF solution at 80 °C: (a) Purged with air and (b) Purged with H_2.

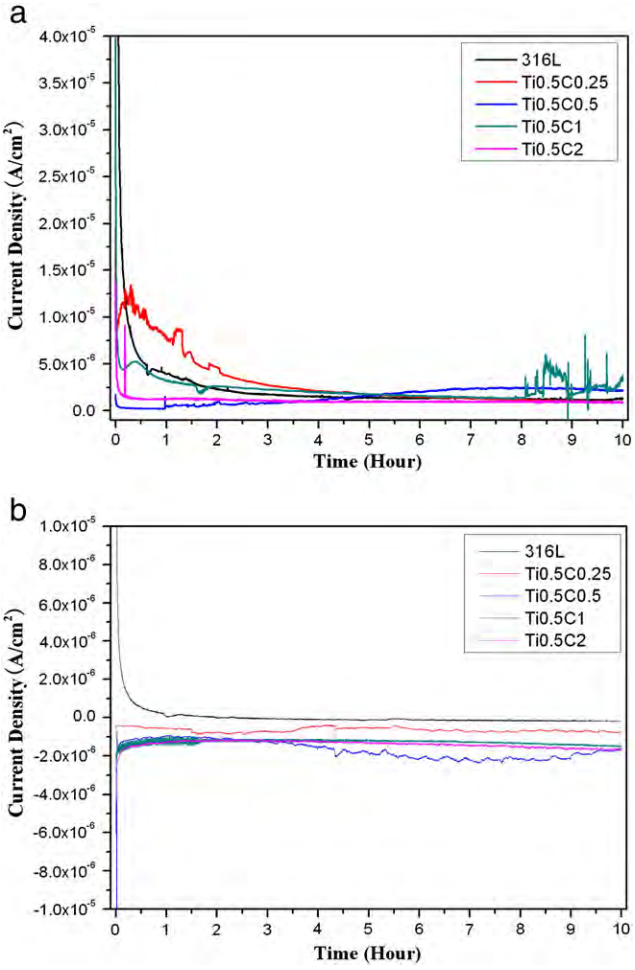

Fig. 7. Potentiostatic curves obtained from the bare and Ti and C implanted SS316L samples: (a) Simulated cathode (0.6 V vs SCE purged with air) and (b) Anode environment (−0.1 V vs SCE purged with H_2).

potential, 0.6 V on the cathode side and −0.1 V on the anode side [4,24]. Fig. 7 shows the potentiostatic curves under the simulated PEMFC conditions. The current density decreases rapidly initially and then gradually stabilizes due to the good passivation ability. Although the passive current density of the bare SS316L is much larger than that of Ti0.5C0.5 as measured by the potentiodynamic test, the current density in the potentiostatic test is almost the same, indicating that the passivation ability of SS316L is better than that of the implanted specimen. Although passivation retards the corrosion rate and prevents the substrate from further corrosion, the surface electrical conductivity is sacrificed thereby decreasing the output power density of PEMFC stack. It is noted that the current density of Ti0.5C1 in Fig. 7 (a) in the end of test is not stable, which indicates that the surface of this sample is unstable and would be corroded with local corrosion. In the simulated anode environment, −0.1 V vs SCE is applied during the potentiostatic test under H_2 purging. The potentiostatic results show very different curves between the unimplanted and implanted SS316L. The bare SS316L exhibits a passivation behavior typical of SS316L in the cathode environment whereas the implanted specimen displays an opposite tendency. It is reasonable that the corrosion potential of the implanted specimen is higher than the applied anodic potential of −0.1 V. The negative current density indicates cathodic protection in this environment.

The SEM micrographs of the implanted SS316L after the potentiostatic tests are depicted in Fig. 8. Only a small part of the surface is corroded. There is no obvious corrosion on the surface of Ti0.5C0.25

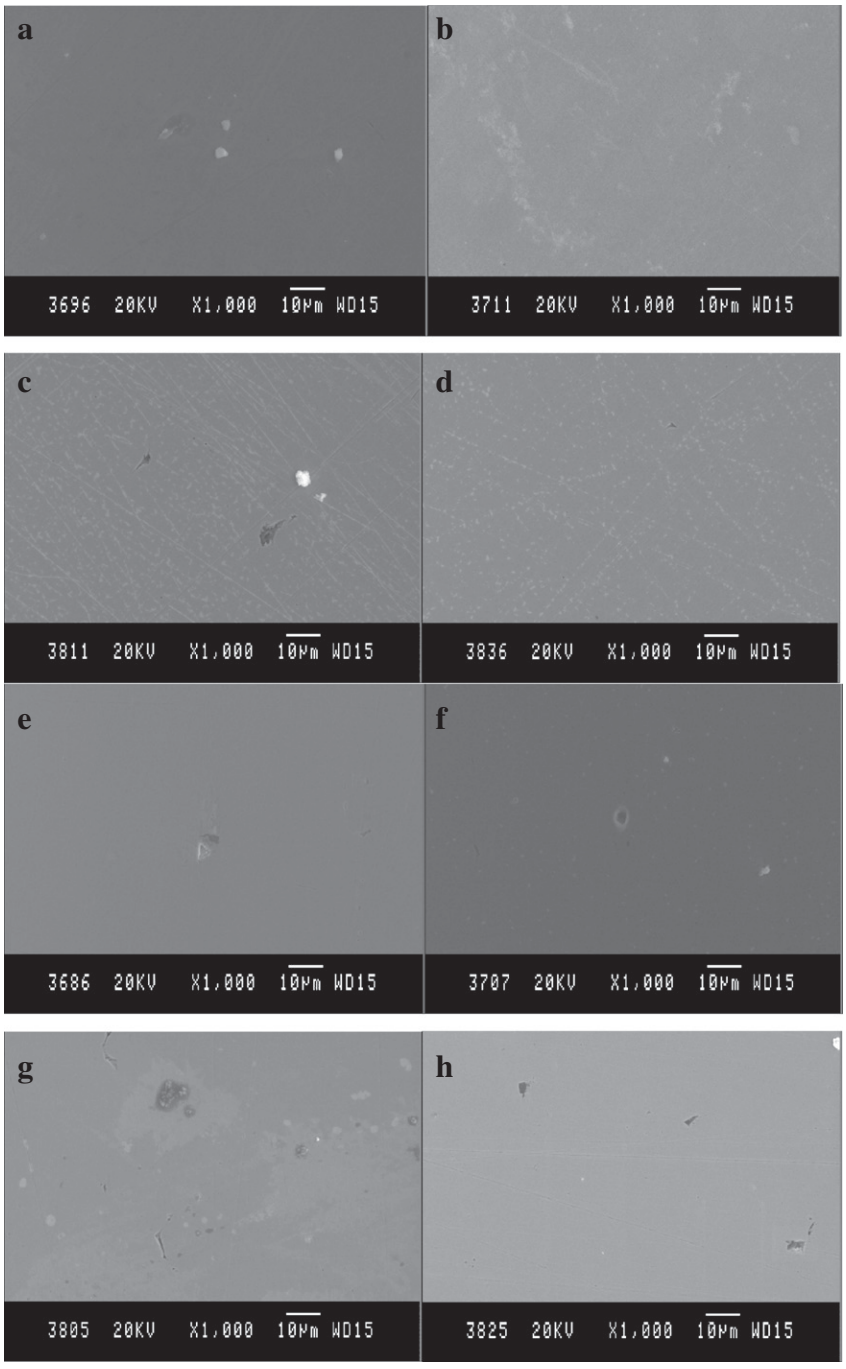

Fig. 8. SEM images of Ti and C implanted specimens after polarization in the PEMFC cathode environment: (a) Ti0.5C0.25, (b) Ti0.5C0.5, (c) Ti0.5C1, (d) Ti0.5C2 and in the PEMFC anode environment: (e) Ti0.5C0.25, (f) Ti0.5C0.5, (g) Ti0.5C1, (h) Ti0.5C2.

and Ti0.5C0.5 after polarization in the cathode environment, whereas localized corrosion can be observed for Ti0.5C1 sample. Local corrosion is apparent in the simulated anode environment due to the presence of H_2, especially on the surface of Ti0.5C1 and Ti0.5C2. Ion implantation will inevitably create defects in the near surface region when entering into the substrate. While the defects on the surface allows hydrogen in the anode environment permeate into the surface more easily, making the sample prone to local corrosion. SEM indicates that a proper ion implant fluence, for example, Ti0.5C0.5 in this case, significantly inhibits the surface corrosion process.

The solutions after the potentiostatic test are collected and the metal ions dissolved were determined by ICP and the results are summarized in Table 2. Fe shows the highest concentration of all dissolved ions in all cases, implying that Fe in the stainless steel is selectively dissolved. This is attributed to higher mobility of iron cations as compared to chromium cations in the passive film [28,29]. For the unimplanted and implanted with lower fluence of SS316L, more metal ions are generated in the cathode environment than in the anode environment, indicating that the cathode environment is more corrosive. It is because that the negative current in the simulated PEMFC anode environment should provide partially cathodic protection. However, the metal ion concentrations leached from Ti0.5C2 sample in the simulated anode environment is found to be more than that in the cathode one, indicating that the implanted samples corrode faster in the anode environment. This is due to the high implantation fluence creating excess tunnels and defects in the near surface region when entering the substrate. Hydrogen in the anode environment thus is more easily to permeate into the surface, forming active sites for the passive film breakdown and pit initiation [30]. The greatest reduction in the ion concentrations in the solution is observed from Ti0.5C0.5 sample. The total metal ion concentration is reduced by 5 times in the cathode environment and 3.3 times in the anode environment, compared to the unimplanted SS316L. These data imply that good corrosion resistance is achieved by proper Ti + C dual implantation fluence. It is also noted that the current density of ion implanted SS316L during potentiostatic test is equal to or larger than that of unimplanted sample in the cathode environment. While the ICP results indicate that ion implanted sample releases less metal ions than the unimplanted one. This is due to the different electrochemical reaction process on the surface of implanted and unimplanted SS316L.

The initial performance of the single cell assembled with the Ti and C implanted and uninplanted stainless steel bipolar plates is shown in Fig. 9. The performance of the PEMFC is affected by the resistance over potential, activation over potential, as well as concentration over potential. In this case, the resistance over-potential is the major factor since the assembling and testing conditions are the same. The open circuit voltage (OCV) of the single cell with the ion implanted bipolar plate is almost the same as that of the bare SS bipolar plates, being 970.7 mV and 979.6 mV, respectively. The peak power density of the single cell assembled with the bare SS bipolar plates is 566.5 mW cm^{-2} at a current density of 1655.2 mA cm^{-2} and the power density at 0.6 V is 299.7 mW cm^{-2}. As for the Ti + C dual implanted bipolar plates, the peak power density is 709.8 mW cm^{-2} at a current density of 1911.9 mA cm^{-2}, while the power density is 443.6 mW cm^{-2} at 0.6 V. The results indicate that the single cell performance is significantly improved by Ti and C ion implantation. As the sweeping current density increases, the output voltage of the single cell with the bare SS bipolar plates decreases faster than that measured from the implanted SS bipolar plates due to a much higher ICR of the unimplanted stainless steel as illustrated in Fig. 5. Therefore, the ICR is a dominant factor affecting the resistance over potential of a single cell.

Table 2
Fe, Cr, Ni, Mo and Ti ion concentrations for the bare and dual Ti and C implanted SS316L in 0.5 M solutions after 10 h potentiostatic test.

Sample	Ion concentration in PEMFC cathode environment after 10 h (ppm)					Ion concentration in PEMFC anode environment after 10 h (ppm)				
	Fe	Cr	Ni	Mo	Ti	Fe	Cr	Ni	Mo	Ti
SS316L	7.62	0.88	0.69	0.08	–	6.28	0.90	0.61	0.15	–
Ti0.5C0.25	2.97	0.29	0.12	0.03	0.03	1.62	0.40	0.20	0.02	0.07
Ti0.5C0.5	1.66	0.11	0.06	0.02	0.02	1.58	0.44	0.23	0.06	0.05
Ti0.5C1	3.81	0.41	0.18	0.04	0.11	3.61	0.43	0.18	0.03	0.46
Ti0.5C2	6.04	1.64	0.54	0.19	0.56	6.90	1.90	0.98	0.24	0.57

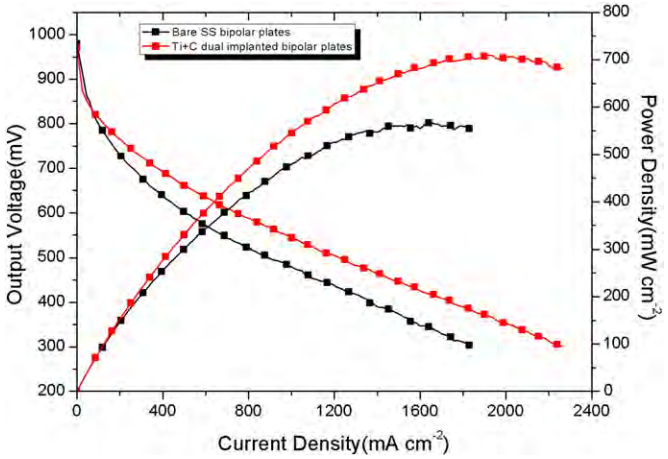

Fig. 9. Single cell performance of the Ti and C implanted and unimplanted SS316L bipolar plates.

4. Conclusion

Dual Ti and C ion implantation is performed to improve the corrosion resistance and surface conductivity of 316L stainless steel bipolar plates used in PEMFC. The corrosion resistance is improved and the ICR is reduced by 6.5 times due to the Ti and C enriched surface. The single cell test also indicates obvious improvement associated with the power density and output voltage. In Ti0.5C0.5, the peak titanium and carbon concentration is 14% and 25%, respectively and an amorphous phase about 32 nm thick with a compact structure and fine-grain underlayer are formed. The ICR and electrochemical test indicate substantial improvement in the surface conductivity and corrosion resistance after ion implantation. In comparison, the cross-sectional microstructure of Ti0.5C2 is composed of a layer containing precipitated nanophases on the surface with an amorphous phase about 22.6 nm thick underneath and a refined grain zone between modified layer and substrate. The proper ion implant fluences, Ti0.5C0.5 in this case, significantly inhibit surface corrosion. Based on the ICR and electrochemical results, ion implantation of titanium for 0.5 h and carbon for 0.5 h are selected to modify SS bipolar plates. The single cell test results show that the peak power density assembled with the ion implanted bipolar plates increases from 566.5 mW cm^{-2} to about 709.8 mW cm^{-2} and the power density at 0.6 V increases by about 50% compared to the single cell assembled with the unimplanted SS bipolar plates.

Acknowledgments

Financial support provided by National Natural Science Foundation of China under contract number 50820125506 and No. 50971091, National High Technology Research and Development Program 863 under contract number 2009AA05Z120, the Ministry of Science and Technology of the People's Republic of China (Grant No. 2009DFB50350), and Hong Kong Research Grants Council (RGC) General Research Funds (GRF) No. CityU 112510 is acknowledged. The authors also thank Linfa Peng, Peiyun Yi, and Diankai Qiu in the School of Mechanical

Engineering, SJTU for their assistance in the ICR and single cell measurements.

References

[1] R.C. Makkus, A.H.H. Janssen, F.A. de Bruijn, R.K.A. Mallant, J. Power. Sources 86 (2000) 274.
[2] D.P. Davies, P.L. Adcock, M. Turpin, S.J. Rowen, J. Power. Sources 86 (2000) 237.
[3] A. Pozio, R.F. Silva, M.D. Francesco, L. Giorgi, Electrochim. Acta 48 (2003) 1543.
[4] H. Wang, M.A. Sweikart, J.A. Turner, J. Power. Sources 115 (2003) 243.
[5] R.A. Antunes, M.C.L. Oliveira, G. Ett, V. Ett, Int. J. Hydrogen Energy 35 (2010) 3632.
[6] P. Yi, L. Peng, L. Feng, P. Gan, X. Lai, J. Power. Sources 195 (2010) 7061.
[7] O. Lavigne, C. Alemany-Dumont, B. Normand, P. Delichère, A. Descamps, Surf. Coat.Technol. 205 (2010) 1870.
[8] X.Y. Liu, P.K. Chu, C.X. Ding, Mater. Sci. Eng. R: Reports 47 (2004) 49.
[9] P.K. Chu, S. Qin, C. Chan, N.W. Cheung, L.A. Larson, Mater. Sci. Eng. R: Reports 17 (1996) 207.
[10] N. Theodoropoulou, A.F. Hebard, S.N.G. Chu, M.E. Overberg, C.R. Abernathy, S.J. Pearton, R.G. Wilson, J.M. Zavada, J. Appl. Phys. 91 (2002) 7499.
[11] A. Anders, Surf. Coat.Technol. 183 (2004) 301.
[12] M.K. Lei, Y.X. Ou, K.S. Wang, L. Chen, Surf. Coat.Technol. 205 (2011) 4602.
[13] M. Xu, L.H. Li, Y.M. Liu, X. Cai, Q.L. Chen, P.K. Chu, Mater. Sci. Eng. A 425 (2006) 1.
[14] T. Zhang, H. Huang, C. Ji, J. Chen, G. Sun, H. Zhang, X. Zhang, Surf. Coat.Technol. 65 (1994) 148.
[15] T. Zhang, Y. Wu, H. Zhang, Z. Deng, G. Zhou, H. Liang, F. Ma, X. Zhang, X. Wang, Nucl. Instrum. Methods Phys. Res., Sect. B 169 (2000) 112.
[16] M.-U. Kim, Kim D-H, S.-H. Han, E. Fleury, H.-K. Seok, P.-R. Cha, Y.-C. Kim, Met. Mater. Int. 17 (2011) 283.
[17] D. Weng, M. Wang, Mater. Chem. Phys. 54 (1998) 338.
[18] G.K. Hubler, P. Trzaskoma, E. McCafferty, I.L. Singer, Ion implantation into metals, Pergamon Press, New York, NY, 1982, p. 24.
[19] G.Y. Yushkov, A. Anders, E.M. Oks, I.G. Brown, J. Appl. Phys. 88 (2000) 5618.
[20] K. Feng, Y. Shen, D. Liu, P.K. Chu, X. Cai, Int. J. Hydrogen Energy 35 (2009) 69.
[21] L. Yang, H. Yu, L. Jiang, L. Zhu, X. Jian, Z. Wang, J. Power. Sources 195 (2010) 2810.
[22] V.V. Nikam, R.G. Reddy, S.R. Collins, P.C. Wiliams, G.H. Schiroky, G.W. Henrich, Electrochim. Acta 53 (2008) 2743.
[23] M. Kumagai, S.T. Myung, R. Asaishi, Y.K. Sun, H. Yashiro, Electrochim. Acta 54 (2008) 574.
[24] Y. Wang, D.O. Northwood, Int. J. Hydrogen Energy 32 (2007) 895.
[25] Z. Yi, Z. Xiao, F. Ma, T. Zhang, Y. Li, Surf. Coat. Technol. 128 (2000) 186.
[26] Z. Yi, F. Xu, F. Ma, T. Zhang, Y. Li, G. Zhou, Surf. Coat. Tech. 131 (2000) 360.
[27] K. Feng, T. Hu, X. Cai, Z. Li, P.K. Chu, J. Power Sources 199 (2012) 207.
[28] R. Kirchheim, B. Heine, H. Fischmeister, S. Hoffman, H. Knote, U. Stolz, Corros. Sci. 29 (1989) 899.
[29] N. Sato, K. Kudo, T. Noda, Corros. Sci. 10 (1970) 785.
[30] A.K. Iversen, Corros. Sci. 48 (2006) 1036.